Computers & Geosciences 168 (2022) 105214

Contents lists available at ScienceDirect

Computers and Geosciences

journal homepage: www.elsevier.com/locate/cageo

Research paper

Constrained non-linear AVO inversion based on the adjoint-state optimization

Nisar Ahmed [a,*], Wiktor Waldemar Weibull [a], Dario Grana [b]

[a] Department of Energy Resources, University of Stavanger, 4021, Stavanger, Norway
[b] Department of Geology and Geophysics, School of Energy Resources, University of Wyoming, Laramie, WY 82071, United States

ARTICLE INFO

Keywords:
AVO inversion
Gradient descent
Adjoint-state method
Objective function
L-BFGS optimization algorithm

ABSTRACT

Pre-stack AVO inversion of seismic data is a modeling tool for estimating subsurface elastic properties. Our focus is on the model-based inversion method where then unknown variables are estimated by minimizing the misfit to the observed data. Standard approaches for non-linear AVO inversion are based on the gradient descent optimization algorithms that require the calculation of the gradient equations of the objective function. To improve the accuracy and efficiency of these methods, we developed a technique that uses an implementation of the adjoint-state-based gradient computation. The inversion algorithm relies on three basic modeling components consisting of a convolution-based forward model using a linearized approximation of the Zoeppritz equation, the definition of the objective function, and the adjoint-computed gradient. To achieve an accurate solution, we choose a second-order optimization algorithm known as the Limited memory-BFGS (L-BFGS) that implicitly approximates the inverse Hessian matrix. This approach is more efficient than traditional optimization methods. The main novelty of the proposed approach is the derivation of the adjoint-state equations for the gradient of the objective function. The application of the proposed method is demonstrated using 1D and 2D synthetic datasets based on data from the Edvard Grieg oil field. The seismic data for these applications is generated by using both convolutional modeling and finite difference methods. The results of the proposed method are accurate and the computational approach is efficient. The results show that the algorithm reliably retrieves the elastic variables, P- and S-wave velocities and density for both convolutional and finite difference models.

1. Introduction

In seismic inversion, the objective is to reconstruct unknown model variables in the subsurface, for example, elastic velocities, from a set of seismic measurements, including seismic amplitudes and travel time measured at the surface (Aki and Richards, 1980). The inversion results are retrieved from seismic reflection data by solving the non-unique and ill-posed inverse problem and they provide a quantitative model of predicted physical properties varying laterally and vertically (Buland and Omre, 2003). Seismic data inversion schemes can be split into two main classes, post-stack (or acoustic) impedance, and pre-stack (or elastic) inversions. Post-stack inversion aims to predict acoustic impedance from stacked seismic data and it is often used in stratigraphic interpretation (Ghosh, 2000) but it does not give any information about the shear wave velocity (Morozov and Ma, 2009; Maurya et al., 2018). On the other hand, pre-stack inversion is based on the concept of amplitude variations with offset/angle (AVO/A) and aims to predict a set of elastic attributes such as seismic velocities, impedances and density (Downton, 2005). AVO inversion results are typically correlated with petrophysical attributes like porosity, saturation of fluids, and reservoir litho-facies. These properties play a significant role in lithology prediction, geofluids identification, and quantitative reservoir characterization (Chiappa and Mazzotti, 2009; Zhao et al., 2014; Luo et al., 2019; Grana, 2020). In addition, AVO inversion can also be used in time-lapse seismic monitoring studies to predict the changes in pressure, saturation, and porosity, as an example, for CO_2 sequestration in depleted reservoirs (Lang and Grana, 2019; Dupuy et al., 2021).

A seismic reflection event at the recording point is described generally by the convolution of the seismic source and the reflectivity series based on the wave equations (Mallick, 2007), Zoeppritz equations (Kurt, 2007; Skopintseva et al., 2011; Liu et al., 2016) or linearized approximations (Aki and Richards, 1980; Buland and Omre, 2003; Buland and El Ouair, 2006; Downton and Ursenbach, 2006; Rabben and Ursin, 2011; Xiao et al., 2020). The inversion can be performed according to deterministic or probabilistic inversion methods.

* Corresponding author.
E-mail address: nisar.ahmed@uis.no (N. Ahmed).

https://doi.org/10.1016/j.cageo.2022.105214
Received 22 December 2021; Received in revised form 22 June 2022; Accepted 5 August 2022
Available online 17 August 2022

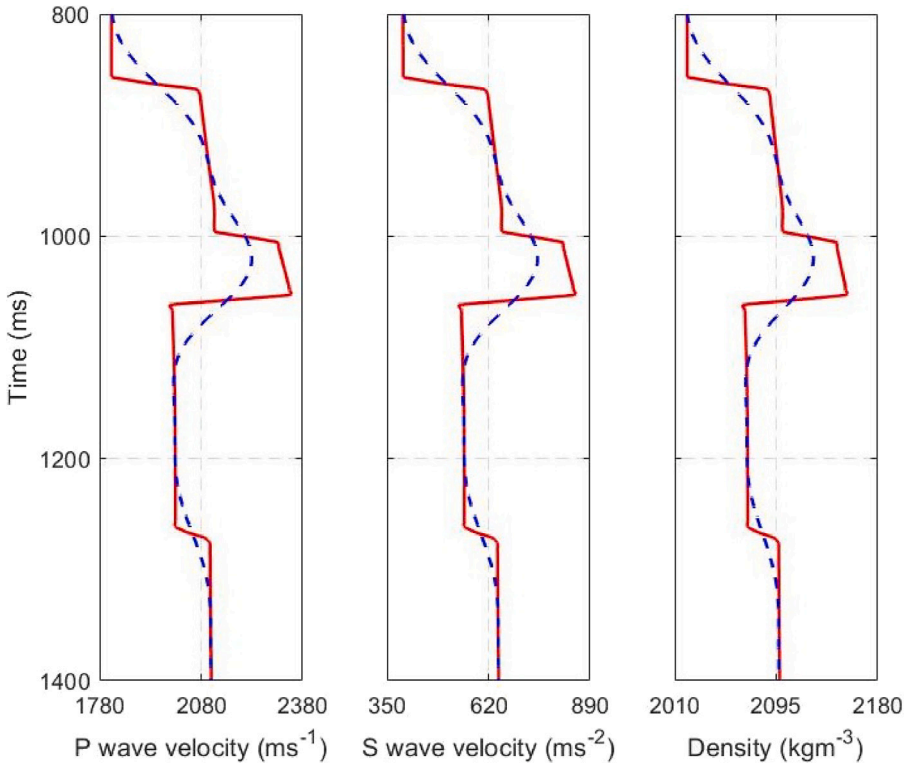

Fig. 1. Example 1 — Model variables (solid red lines): the P and S wave velocities in (m/s) and the bulk density in (kg m^{-3}) and the corresponding initial guesses (dashed blue lines) at the well location in the TWT interval 800–1400 ms are plotted in the figure.

For example, based on Aki and Richards linearized approximation, Hu et al. (2011) presents a joint AVO inversion technique in the Bayesian framework to extract seismic velocities and density parameters, Sengupta et al. (2021) perform Bayesian inversion directly in the depth domain by using linearized Aki and Richards equation, and Liu et al. (2021) present a joint PP and PS inversion method based on the calculation of a Jacobian matrix of the Zoeppritz approximation. In addition to gradient-based optimization, the Monte Carlo inversion method (Jin and Madariaga, 1994) and Bayesian linearized AVO inversion technique based on Gaussian distributions (Tarantola, 1987; Buland and Omre, 2003) have also been utilized to solve the inverse problems and quantify the uncertainty of the predicted model. Feng-Qi et al. (2013) present a Bayesian linearized pre-stack inversion based on a trivariate Cauchy distribution. Ensemble-based methods such as ensemble Kalman filter and ensemble smoother (Evensen et al., 2009) have been successfully applied to inverse and data assimilation problems, especially for history matching of borehole and geophysical data. For example, Luo et al. (2015) developed an iterative ensemble smoother based on a regularized Levenberg–Marquardt (RLM) algorithm for reservoir data assimilation, and Luo et al. (2017) applied the iterative ensemble smoother to 4D-seismic history-matching. Kolbjørnsen et al. (2020) develop a Bayesian inversion for litho-geofluids prediction and Grana (2020) extends the Bayesian litho-geofluids approach to multiple prior models. Bayesian methods can also be integrated with stochastic sampling. For example, Azevedo et al. (2020) uses the stochastic perturbation optimization approach for the inversion of seismic data for rock properties and facies. In the Bayesian method, prior information about the subsurface model is included in the inversion in the form of probability distributions (Gouveia and Scales, 1997). However, the prior information is often difficult to define and the prior uncertainty generally impacts the model predictions.

In deterministic methods, the goal is to predict a best-fit model that is consistent with the observed data, according to the objective or cost function that defines the dissimilarity between the true data and the predicted model. The inversion is performed by searching for the optimal model that minimizes the objective function. Numerous iterative algorithms such as the Levenberg–Marquardt (LM) algorithm (Levenberg, 1944; Marquardt, 1963), Occam's inversion (Constable et al., 1987), genetic algorithm (Mallick, 1995), conjugate gradient method (Golub and Van Loan, 2013), simulated annealing method (Ma, 2001) and particle swarm optimization (Shaw and Srivastava, 2007) have been introduced for solving the least-squares optimization problems. These methods have been used in seismic AVO inversion problems. For example, Luo et al. (2020a,b) adopt the Fréchet derivatives to compute the derivatives of the propagator matrix with respect to variables and used the L-BFGS approach for the optimization of the objective function.

In this work, we present a constrained non-linear AVO inversion scheme by using the Aki and Richards linearized approximation and the inversion algorithm is based on the minimization of an objective function. We adopt a gradient descent optimization algorithm depending on the calculation of the gradients of the L2-norm objective function with respect to the elastic properties, P- and S-wave velocities, and density. The adjoint-state numerical technique (Plessix, 2006) is used for computing the gradients of the objective function efficiently by employing zero-lag cross-correlation between forward and reverse propagated data residual. The adjoint-state solves a linear system and computes the gradient of the objective function. The advantage of this method is that the computational cost of computing the gradient is in practice independent of the number of model variables (N). Hence, the number of forwarding models required to compute the gradients through the adjoint-state method is independent of the number of unknown model variables. This makes adjoint-state faster and more efficient than other methods, such as finite difference and Fréchet derivatives (Plessix, 2006). Adjoint methods have been recently used in several geophysical inversion problems including seismic full waveform inversion (Zheglova and Malcolm, 2019; Pan et al., 2020; Le et al., 2020; Biondi et al., 2021; Assis and Schleicher, 2021; Hu et al., 2021; Zhu et al., 2021; Ravasi and Vasconcelos, 2021). Furthermore, the gradient equations obtained via the adjoint-state technique are exact within the numerical

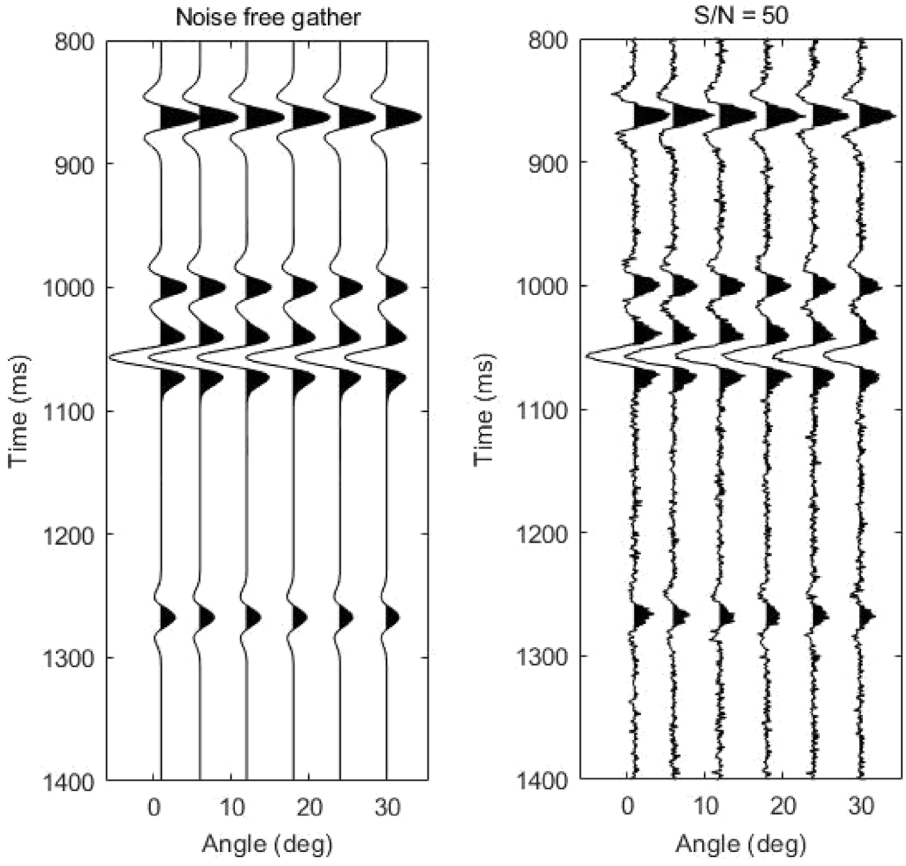

Fig. 2. Example 1 — Pre-stack amplitude versus angle (AVA) gathers with different seismic noise levels (without and with S/N = 50) up to maximum incident angle 30°.

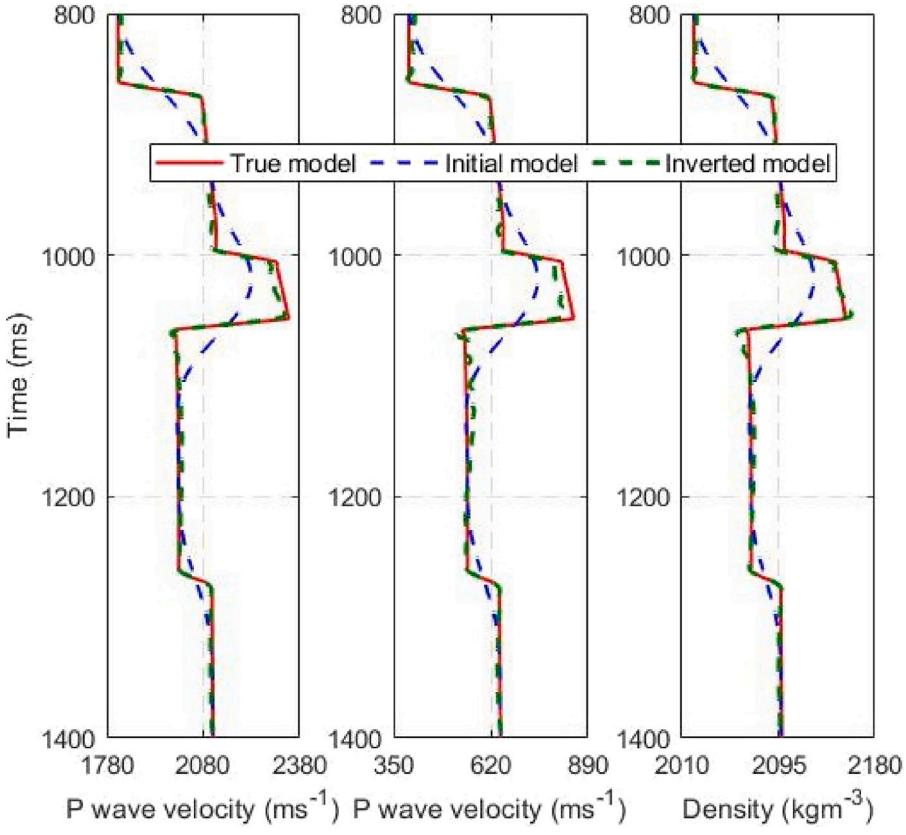

Fig. 3. Example 1 — Inverted P- and S-wave velocities (V_P, V_S) and density (ρ) models obtained from noise-free AVO gathers.

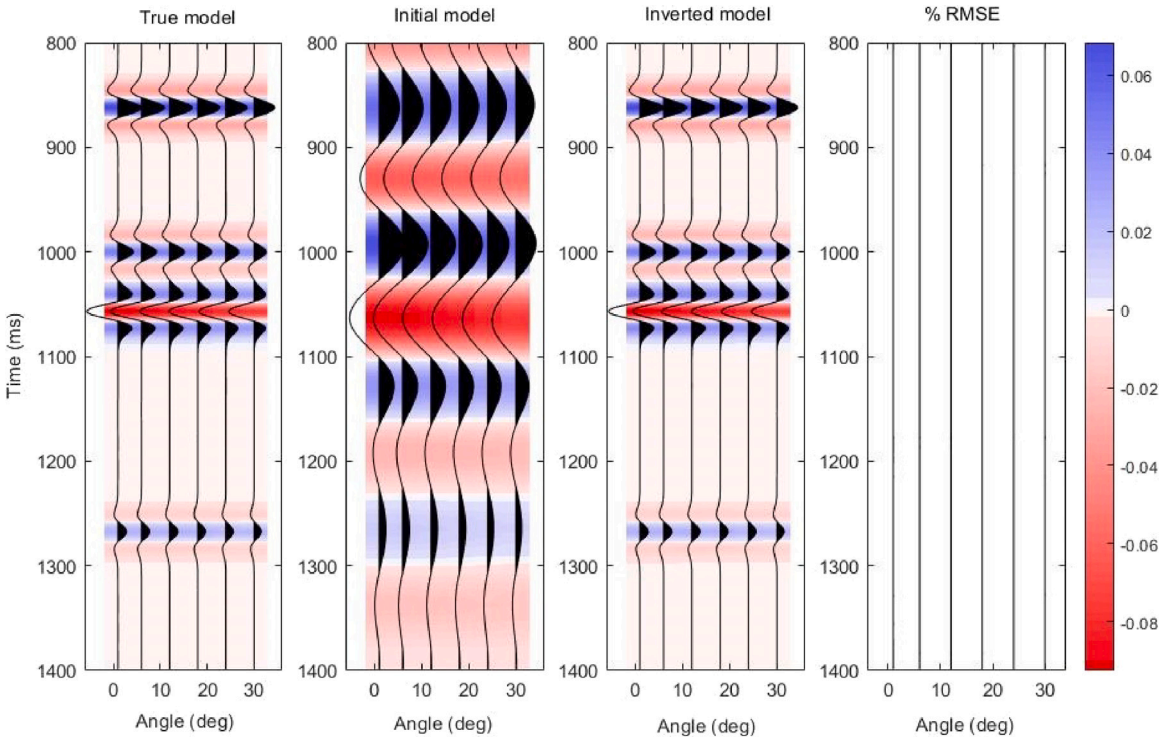

Fig. 4. Example 1 — AVA seismic response (up to 30°) for baseline true model, initial model, and inverted model and estimated RMS error.

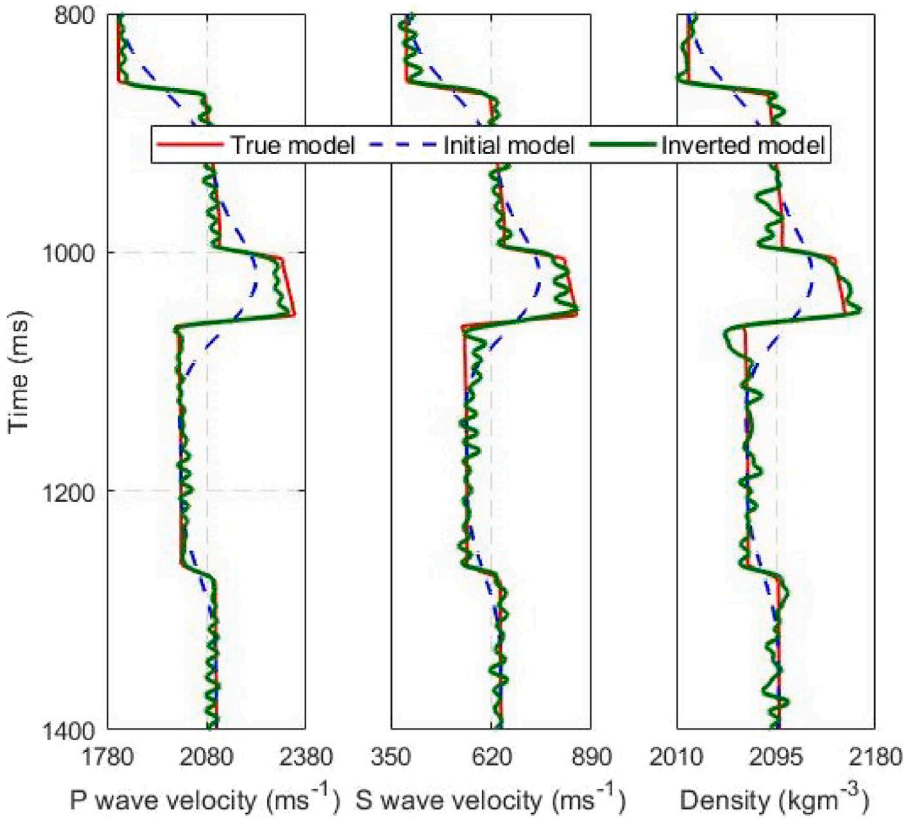

Fig. 5. Example 1 — Inverted P- and S-wave velocities (V_P, V_S) and density (ρ) models obtained from noisy (S/N = 50) seismic AVO gather.

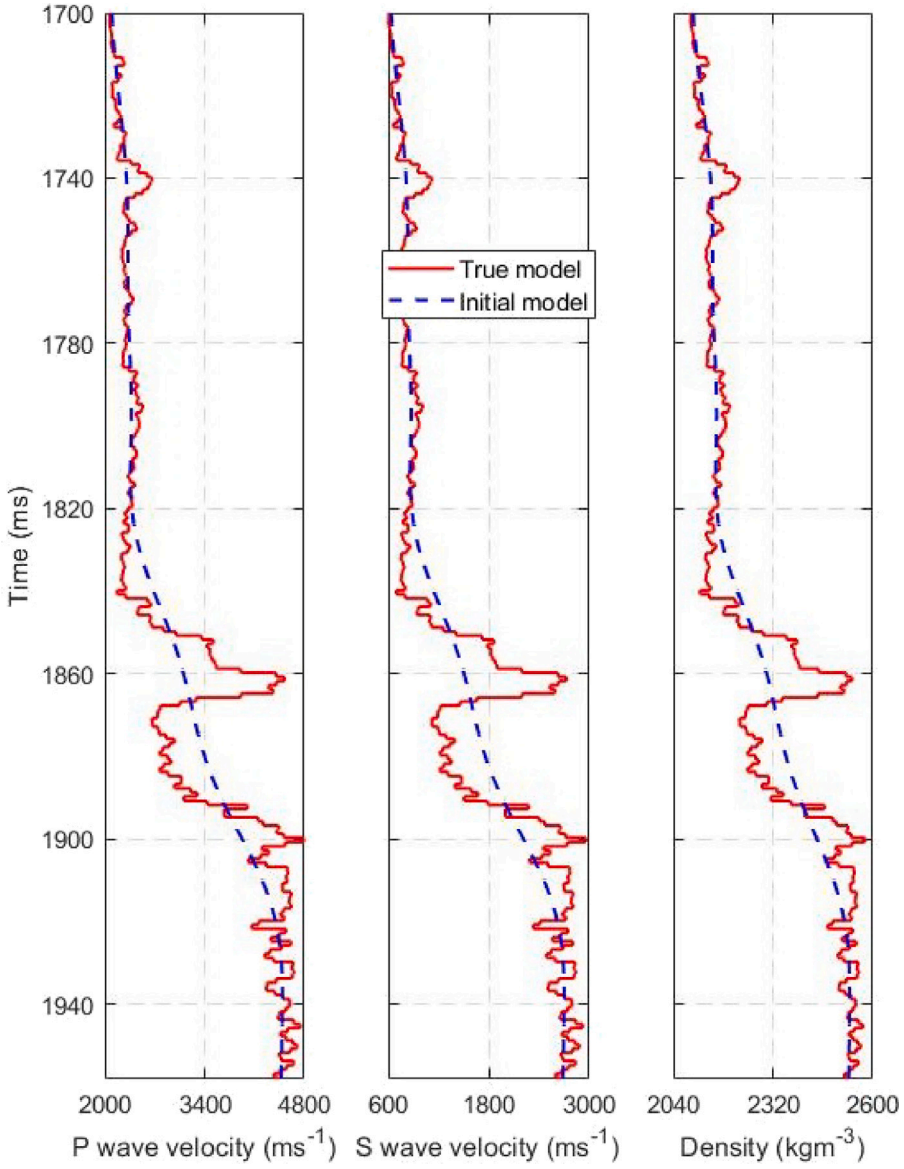

Fig. 6. Example 2 — Model variables: P and S wave velocities in (m/s) and bulk density in (kg m^{-3}) along with corresponding initial models at the well location in the TWT interval 1700–1965 ms.

precision (Epelle and Gerogiorgis, 2020). In this work, to minimize the L2-norm objective function, we use the L-BFGS method (Broyden, 1970; Fletcher, 1970; Goldfarb, 1970; Shanno, 1970; Nocedal, 1980; Liu and Nocedal, 1989), a widely used version of the quasi-Newton iteration method that does not explicitly calculate the Hessian operator, which reduces the computing time and memory storage unlike other classical iterative methods such as Newton–Raphson or Gauss–Newton methods (Tarantola, 2005). Indeed, the L-BFGS method exclusively stores model information from a limited number of previous l iterations (usually $l \leq 10$) and provides much faster computational time and improved convergence rates for geophysical inverse problems (Brossier et al., 2010). The main novelty of the proposed approach is the calculation of the gradient of the objective function with respect to the elastic properties using the adjoint-state method. The analytical derivatives computed by the adjoint-state lead to advantages in computational and numerical performance. To stabilize our AVO inversion results, especially in the case of noisy data, we apply a Tikhonov regularization method (Aster et al., 2018). The Tikhonov regularization weights improve the stability of the solution and the accuracy of the optimal model.

We tested the proposed approach using synthetic well logs and seismic data generated for the Edvard Grieg oil field, in the North Sea, with different noise levels. We also adopt the staggered-grid finite difference (FD) method (Virieux, 1986) to simulate the seismic response. The FD approach contains wave propagation effects such as seismic refraction, reflection, multiple reflections, and offset-dependent geometrical spreading. To reconcile the results of the convolutional approximation, we define an amplitude scaling factor that compensates for the effects of offset-dependent geometrical spreading and provides a good match between the two seismic modeling approaches.

In the following, we first discuss the seismic forward modeling approaches including, the convolutional model and finite difference method. Then, we describe the mathematical formulation for the proposed non-linear inversion algorithm based on the adjoint-state technique. Next, we illustrate the implementation of the inversion algorithm to a synthetic multilayered dataset, with and without seismic noise, obtained from well logs assuming no multiples nor other wave propagation effects. Then, a 2D synthetic data example with complex structural features such as inclined strata and fault, is presented. Finally, we apply the approach to a synthetic dataset based

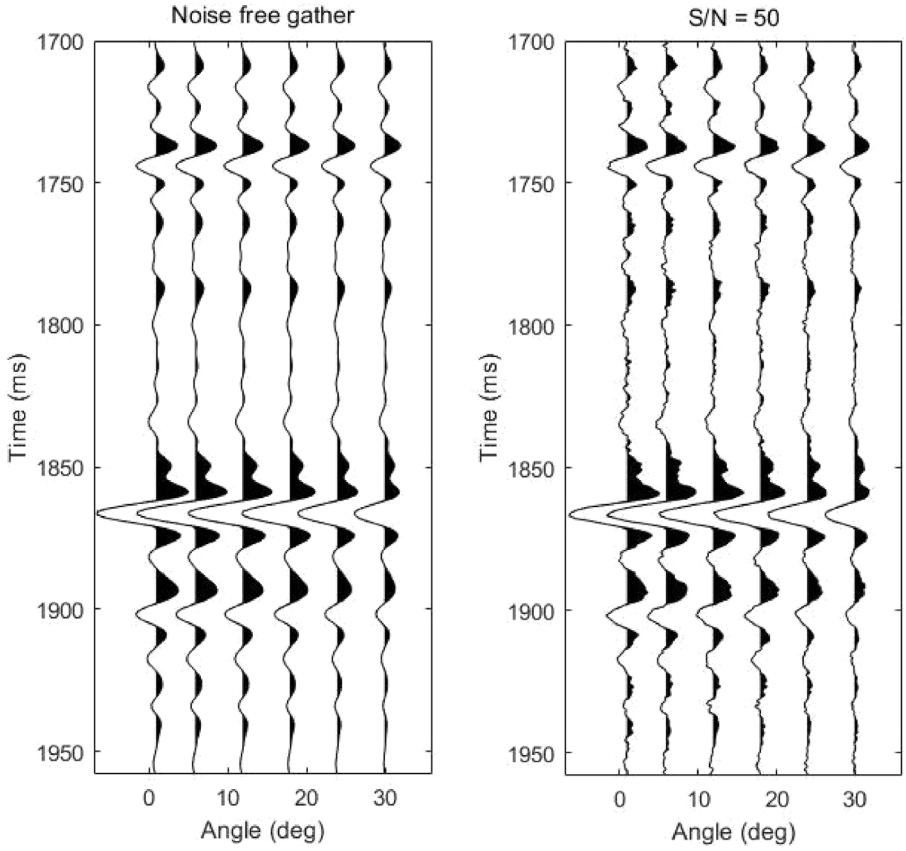

Fig. 7. Example 2 — Pre-stack amplitude versus angle (AVA) gathers with different seismic noise levels (without and with S/N = 50) up to maximum incident angle 30°.

on the velocity–stress finite difference (FD) model, including wave propagation effects.

2. Method

2.1. Seismic modeling

In AVO studies, seismic amplitudes are approximated by a convolutional model. In continuous form, the convolutional model is written as:

$$d(t,\theta) = \int W(\tau,\ \theta) R_{PP}(t-\tau,\ \theta) d(\tau) \tag{1}$$

where d, R_{PP} and W are the seismic data, reflectivity, and wavelet respectively. In Eq. (1), t is the two-way travel time (TWT), and θ is the incident angle. This approximation does not consider multiples and wave propagation effects like offset-dependent geometrical spreading, attenuation, or absorption effects. The Ricker wavelet (Ricker, 1953) is commonly used for the convolutional model:

$$W(t) = \left(1 - \frac{1}{2}\omega_\circ^2 t^2\right) \exp\left(-\frac{1}{4}\omega_\circ^2 t^2\right) \tag{2}$$

whereas $\omega_\circ$ is the dominant frequency. The reflectivity function R_{PP} represents the reflection coefficients of P-to-P waves as a function of t and θ and is often modeled using Aki and Richards equation (Aki and Richards, 1980), which is a linear approximation of the non-linear Zoeppritz equation (Zoeppritz, 1919) for weak elastic contrasts across the geological layers. For incident angles less than the acquisition critical angle, the Aki and Richards equation provides an accurate approximation of the reflection coefficients for small elastic contrasts. In theory, the proposed methodology could be extended to the Zoeppritz equation, however, the analytical evaluation of the mathematical formulation of the gradient is more challenging to derive. The discrete version of Aki and Richards approximation for R_{PP} is:

$$\begin{aligned} R_{PP_{[i]}}(\theta) = &\frac{1}{2}\left(1+\tan^2\theta\right)\frac{\Delta\alpha[i]}{\alpha[i]} - 4\left(\frac{\beta[i]}{\alpha[i]}\right)^2 \frac{\Delta\beta[i]}{\beta[i]}\sin^2\theta \\ &+\frac{1}{2}\left[1 - 4\left(\frac{\beta[i]}{\alpha[i]}\right)^2 \sin^2\theta\right]\frac{\Delta\rho[i]}{\rho[i]} \end{aligned} \tag{3}$$

where $\Delta\alpha$, $\Delta\beta$, and $\Delta\rho$ are the variations P- and S-wave velocities and density across the reflecting interface i whereas α, β and ρ are the corresponding average P- and S-wave velocities and density.

Alternatively, the seismic response can be modeled by solving the wave equation. The finite difference (FD) method is often adopted to approximate the partial derivatives of the wave equation and compute the propagation of seismic waves (Carcione et al., 1988). Several numerical schemes have been proposed. In this work, we adopt a high order (8th) staggered-grid FD scheme (Virieux, 1986) to numerically model in a discretized grid the P-SV elastic seismic energy propagating through a heterogeneous medium using the velocity–stress field. At the time 0, the wave propagating medium is considered to be in equilibrium; then time-integrated particle velocity and stress are propagated. Absorbing boundary conditions (ABCs) are generally assumed for the mathematical simulation of seismic wave propagation, to avoid artificial boundary reflection (ABR). In our approach, we consider a perfectly matched layer (PML) to attenuate modeling boundary reflections. The numerical formulation for the velocity–stress FD method is given by Virieux (1986). In this work, we adopt this formulation to compute a synthetic dataset with a different operator than the convolutional model used for the inversion, to validate the proposed formulation.

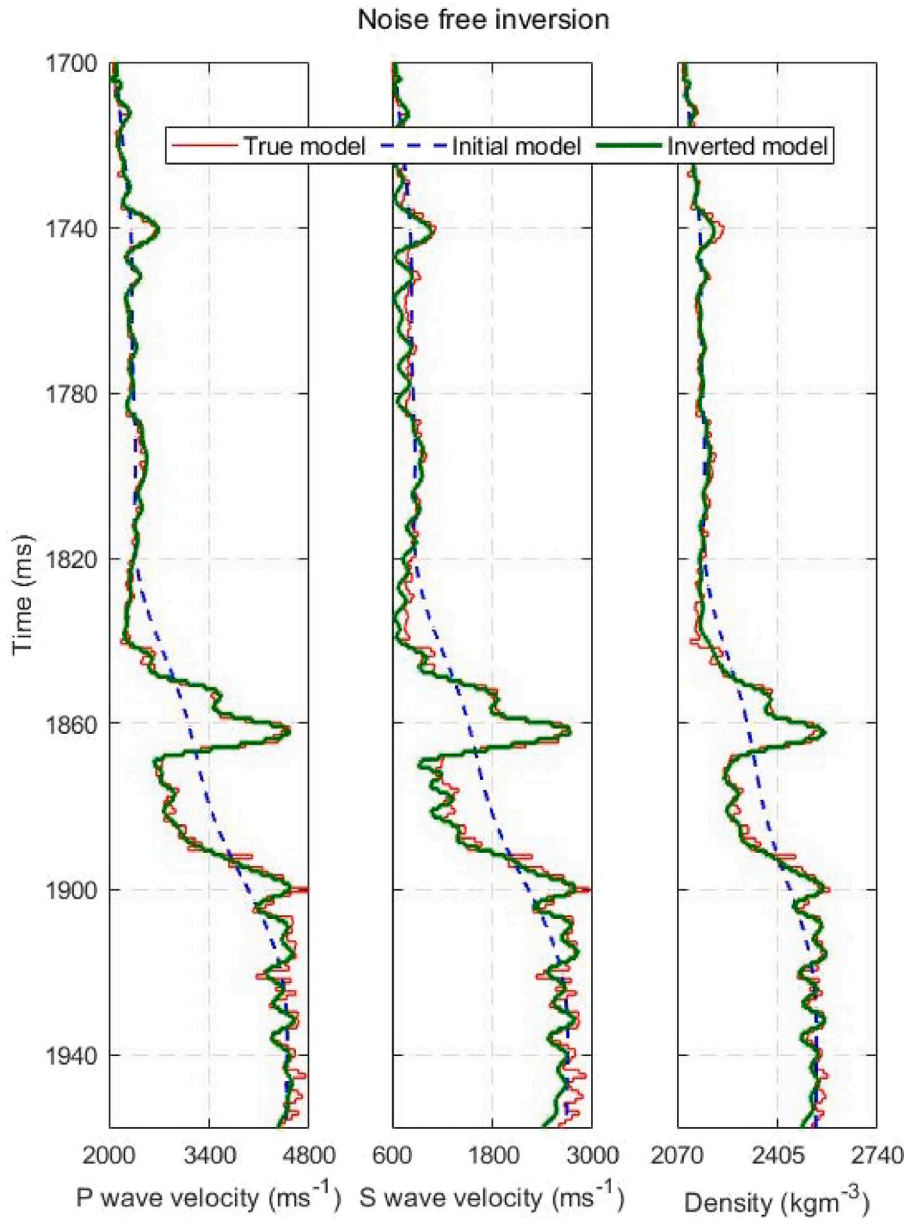

Fig. 8. Example 2 — Inverted P- and S-wave velocities (V_P, V_S) and density (ρ) models obtained from noise-free AVO gathers.

2.2. AVO inversion

The forward modeling equation of seismic AVO inversion is written as $f(m) = d$, where m represents the unknown model variables. The objective of inverse modeling is to estimate the model variables m from the seismic AVO data d. In the proposed formulation, m represents the elastic model variables as $m = [V_P(t), V_S(t), \rho(t)]$, including P- and S-wave velocities and density.

To solve the inverse problem, we first define an objective function to model the misfit $J = d - f(m)$ between the real and predicted data, and then implement an optimization algorithm to minimize the objective function. Numerous options for the definition of the objective functions are available in the literature (Alessandrini et al., 2019; Faucher et al., 2019). We use the Euclidean norm ($L2$-norm), as it is widely used in inversion, especially for problems with a natural scattering of the error components. Mathematically, the $L2$-norm objective function is written as:

$$J(m) = \frac{1}{2}\|d(t,\,\theta) - f(m)\|^2 \tag{4}$$

In our approach, the forward modeling operator is given by the convolutional model:

$$f(m) = W(t) * R_{PP}(t,\,\theta|m) + n(t,\,\theta) \tag{5}$$

here, the term n represents the random ambient noise and * indicates convolution.

The optimization requires the calculation of the partial derivatives of the gradient $\left(\frac{\partial J}{\partial V_P}, \frac{\partial J}{\partial V_S}, \frac{\partial J}{\partial \rho}\right)$ of the objective function J with respect to elastic properties (V_P, V_S, ρ). We adopt the adjoint-state technique to calculate the gradient of the objective function. The adjoint-state solution of Aki and Richards equation (1980) and derivation of the gradient is given in Appendix A. The so-obtained partial derivatives with respect to (V_P, V_S, ρ) at a given interface i are:

$$\begin{aligned}\frac{\partial J}{\partial V_P[i]} &= \frac{1}{2}\left(1+\tan^2\theta\right)\left[-\frac{1}{\alpha[i]} - \frac{\Delta\alpha[i]}{2\alpha[i]^2}\right]\cdot\lambda[i] \\ &+ \frac{1}{2}\left(1+\tan^2\theta\right)\left[\frac{1}{\alpha[i-1]} - \frac{\Delta\alpha[i-1]}{2\alpha[i-1]^2}\right]\cdot\lambda[i-1] \\ &+ \left(\frac{2\beta[i-1]^2}{\alpha[i-1]^3}\right)\left[2\frac{\Delta\beta[i-1]}{\beta[i-1]} + \frac{\Delta\rho[i-1]}{\rho[i-1]}\right]\cdot\sin^2\theta\cdot\lambda[i-1]\end{aligned}$$

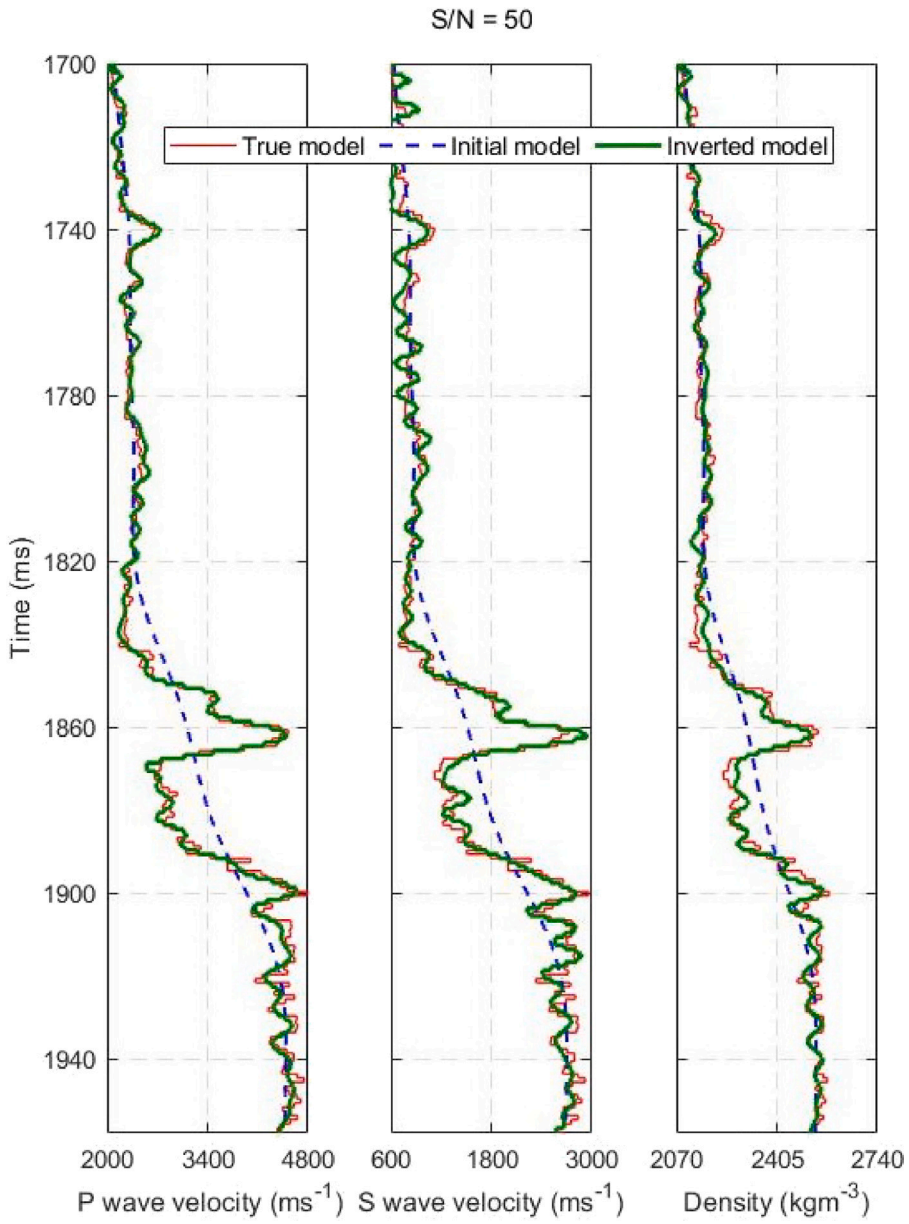

Fig. 9. Example 2 — Inverted P- and S-wave velocities (V_P, V_S) and density (ρ) models obtained from noisy (S/N = 50) seismic AVO gather.

$$+\left(\frac{2\beta[i]^2}{\alpha[i]^3}\right)\left[2\frac{\Delta\beta[i]}{\beta[i]}+\frac{\Delta\rho[i]}{\rho[i]}\right]\cdot\sin^2\theta\cdot\lambda[i], \tag{6}$$

$$\begin{aligned}\frac{\partial J}{\partial V_S[i]} &= \left[-\frac{2\Delta\beta[i-1]}{\alpha[i-1]^2}-\frac{4\beta[i-1]}{\alpha[i-1]^2}\right]\cdot\sin^2\theta\cdot\lambda[i-1]\\ &-\left[\frac{2\Delta\beta[i]}{\alpha[i]^2}-\frac{4\beta[i]}{\alpha[i]^2}\right]\cdot\sin^2\theta\cdot\lambda[i]\\ &-\left[\frac{2\beta[i-1]}{\alpha[i-1]^2}\cdot\frac{\Delta\rho[i-1]}{\rho[i-1]}\right]\cdot\sin^2\theta\cdot\lambda[i-1]\\ &-\left[\frac{2\beta[i]}{\alpha[i]^2}\cdot\frac{\Delta\rho[i]}{\rho[i]}\right]\cdot\sin^2\theta\cdot\lambda[i]\end{aligned} \tag{7}$$

and

$$\begin{aligned}\frac{\partial J}{\partial\rho[i]} &= +\frac{1}{2}\left[1-4\left(\frac{\beta[i-1]}{\alpha[i-1]}\right)^2\cdot\sin^2\theta\right]\left[\frac{1}{\rho[i-1]}-\frac{\Delta\rho[i-1]}{2\rho[i-1]^2}\right]\cdot\lambda[i-1]\\ &-\frac{1}{2}\left[1-4\left(\frac{\beta[i]}{\alpha[i]}\right)^2\cdot\sin^2\theta\right]\left[\frac{1}{\rho[i]}+\frac{\Delta\rho[i]}{2\rho[i]^2}\right]\cdot\lambda[i]\end{aligned} \tag{8}$$

We then apply a non-linear optimization algorithm, namely L-BFGS, to update the model variables by minimizing the objective function J according to the L-BFGS iteration Eq. (9). L-BFGS is a limited-memory quasi-Newton optimization method often used for solving large-scale non-linear optimization problems where the Hessian cannot be efficiently computed. The L-BFGS optimization method iteratively approximates the inverse Hessian using the curvature information from the previous iterations. The L-BFGS optimization method can be represented as:

$$m_{k+1} = m_k - \alpha_k H_k \nabla J, \qquad k = 0, 1, 2, 3, \ldots, \tag{9}$$

where k represents the iteration, α_k is the scalar step length at iteration k, ∇J is the gradient of the objective function respectively, and H_k describes the inverse Hessian approximation ($H_k \approx \nabla^2 J^{-1}$) at iteration k. The inverse Hessian H_k is approximated as:

$$H_{k+1} = V_k^T H_k V_k + \rho_k s_k s_k^T \tag{10}$$

where $V_k = I - \rho_k y_k s_k^T$, $s_k = m_{k+1} - m_k$, $y_k = \nabla J(m_{k+1}) - \nabla J(m_k)$, and $\rho_k = (y_k^T s_k)^{-1}$.

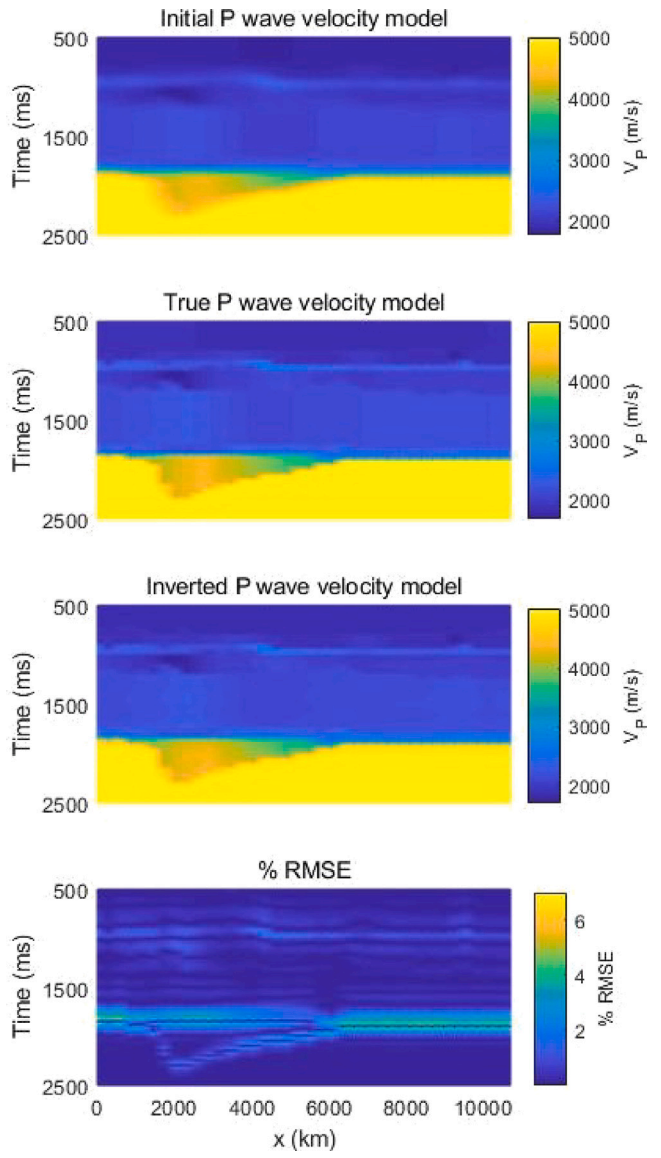

Fig. 10. 2D profile of inverted P-wave velocity compared to the true and initial models. The RMS error between true and inverted models is also displayed.

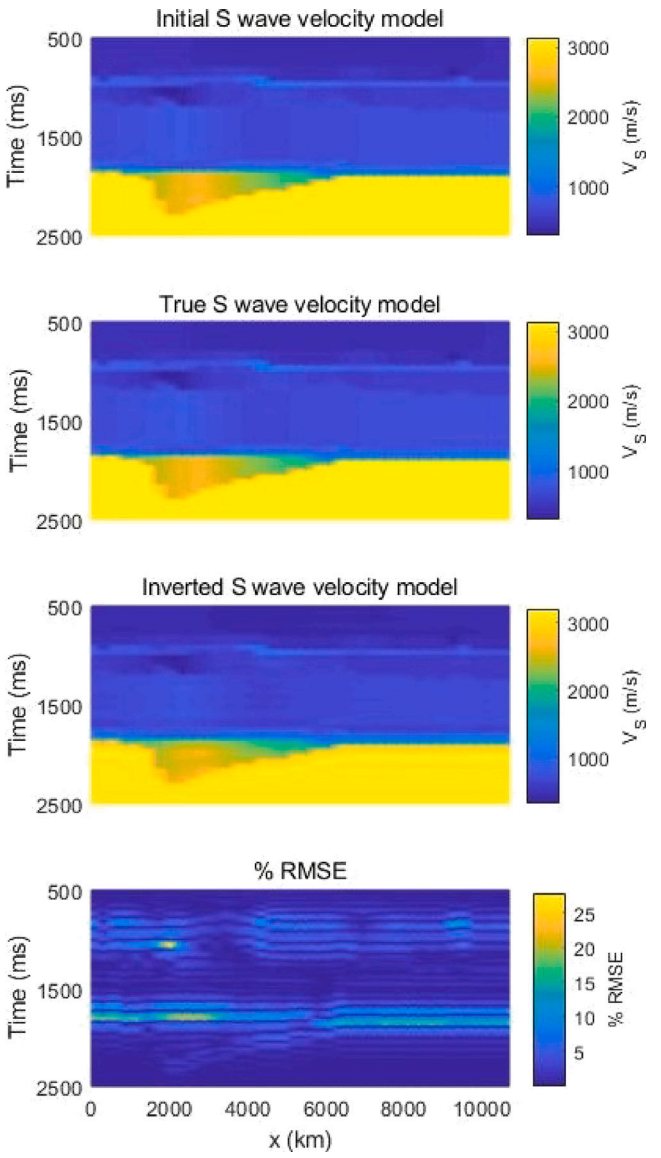

Fig. 11. 2D profile of inverted S-wave velocity compared to the initial and true models. The RMS error is also displayed.

In the L-BFGS method, the Hessian approximation is more efficient than in the original BFGS method. At a given iteration k, suppose that the current solution is m and the vector pairs of the previous p iterations are $\{s_i, y_i\}$ for $i = k-p, \ldots, k-1$ with associated matrices V_i and scalars ρ_i. We choose an initial H_k° and compute H_k as

$$\begin{aligned} H_k = &\left(V_{k-1}^T \ldots V_{k-p}^T\right) H_k^\circ \left(V_{k-p} \ldots V_{k-1}\right) \\ &+ \rho_{k-p}\left(V_{k-1}^T \ldots V_{k-p+1}^T\right) s_{k-p} s_{k-p}^T \left(V_{k-p+1} \ldots V_{k-1}\right) \\ &+ \rho_{k-p+1}\left(V_{k-1}^T \ldots V_{k-p+2}^T\right) s_{k-p+1} s_{k-p+1}^T \left(V_{k-p+2} \ldots V_{k-1}\right) \\ &+ \cdots \\ &+ \rho_{k-1} s_{k-1} s_{k-1}^T \end{aligned} \tag{11}$$

We then define a recursive procedure to efficiently calculate the product $H_k \nabla J_k$, as shown in Algorithm 1.

Algorithm 1: Limited-memory BFGS two-loops recursion.

1. **Inputs:** $\nabla J_k, H_k$
2. $q \leftarrow \nabla J_k$
3. **for** $i = k-1, k-2, \ldots, k-p$ **do**
4. $\alpha_i \leftarrow \rho_i s_i^T q$;
5. $q \leftarrow q - \alpha_i y_i$;
6. **end (for)**
7. $r \leftarrow H_k^o q$
8. **for** $i = k-p, k-p+1, \ldots, k-1$ **do**
9. $\beta_i \leftarrow \rho_i y_i^T r$;
10. $r \leftarrow r + s_i(\alpha_i - \beta)$;
11. **end (for)**
12. **Stop** with result $H_k \nabla J_k = r$

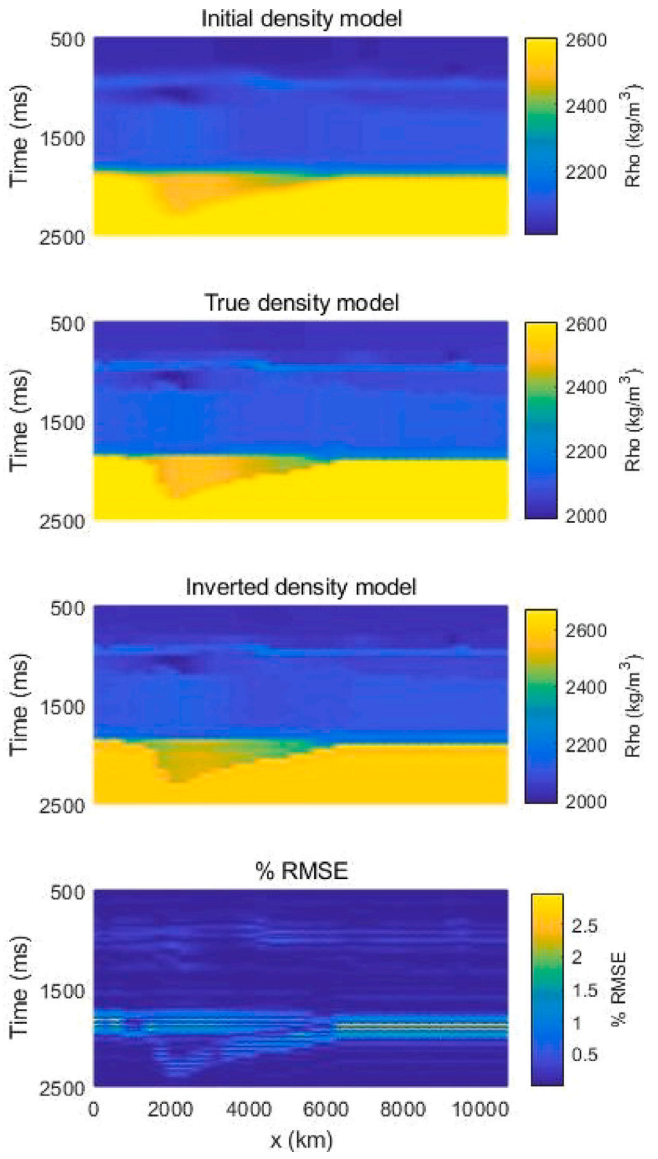

Fig. 12. 2D profile of inverted density compared to the initial and true models. The RMS error between the true and predicted models is also displayed.

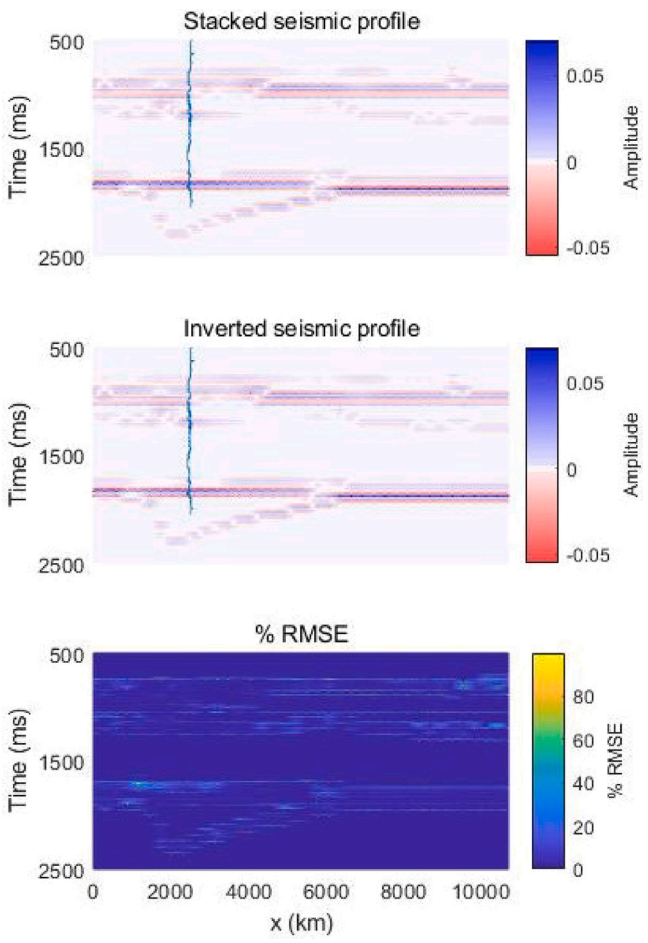

Fig. 13. Full stack seismic section compared to the seismic response of the inverted seismic profile and RMS between real and inverted seismic profiles.

3. Applications

We present numerous numerical examples of synthetic and field datasets used to validate the proposed inversion using the traditional convolutional model. We then extend the application to a synthetic dataset generated using the FD method. Two synthetic subsurface profiles, namely example 1 and example 2, are generated from well logs using the convolutional model. Then the inversion is extended to synthetic 2D data generated from an elastic model developed for the Edvard Grieg oil field located in the North Sea.

In example 1, we use a multilayered convolution model to simulate the synthetic angle gathers from a set of synthetic well log data. S-wave velocity and density are computed from P-wave velocity using Castagna's relation (Castagna et al., 1985) and Gardner's equation (Gardner et al., 1974) respectively. The true model variables and the initial guesses are shown in Fig. 1. Synthetic AVO seismic gathers up to the maximum angle of incidence 30° are generated by convolving a 25 Hz Ricker seismic wavelet with PP reflectivity series calculated with the linearized Aki and Richards equation. The pre-stack angle gather profiles without and with seismic random noise levels (S/N = 50) are shown in Fig. 2. Fig. 3 represents the inverted P wave velocity, S wave velocity, and density from noise-free AVO seismic gather. The inverted variables are in good agreement with the true model variables. Fig. 4 shows the corresponding seismic response of the true, initial and inverted models as well as the root mean square (RMS) error between true and predicted seismic gathers. The inversion results prove the accuracy of this inversion approach. The AVO inversion results with a signal-to-noise ratio (S/N) of 50 are shown in Fig. 5. The inversion results show a good agreement and are consistent with real models, despite some little instability of the solution at quite a few points, especially for S-wave velocity. We speculate that the local instability of the solution might be due to the discrete nature of the model and the band-limited nature of the data. The local instability can be mitigated using a regularization method such as the total variation regularization.

We then test the inversion using a synthetic seismic dataset generated from high-frequency acoustic and shear sonic logs and density data, measured in the Edvard Grieg oil field. These reference elastic properties V_P, V_S, and ρ along with initial models are shown in Fig. 6. The presented true well log measurements (Fig. 6) are upscaled to estimate the model variables at the seismic scale (i.e. seismic wavelet scale) from the higher frequency properties (i.e. sonic log). The reservoir zone is located between 1867 and 1888 ms. The convolution-based seismic forward modeling is used to generate pre-stack seismic AVA gathers (Fig. 7) without noise and with S/N = 50. The range of angles of the incident for seismic waves is from 0–30° with the interval of 5°. Figs. 8 and 9 show the AVA inversion results without and with noise. In the noise-free case, the comparison between true and inverted

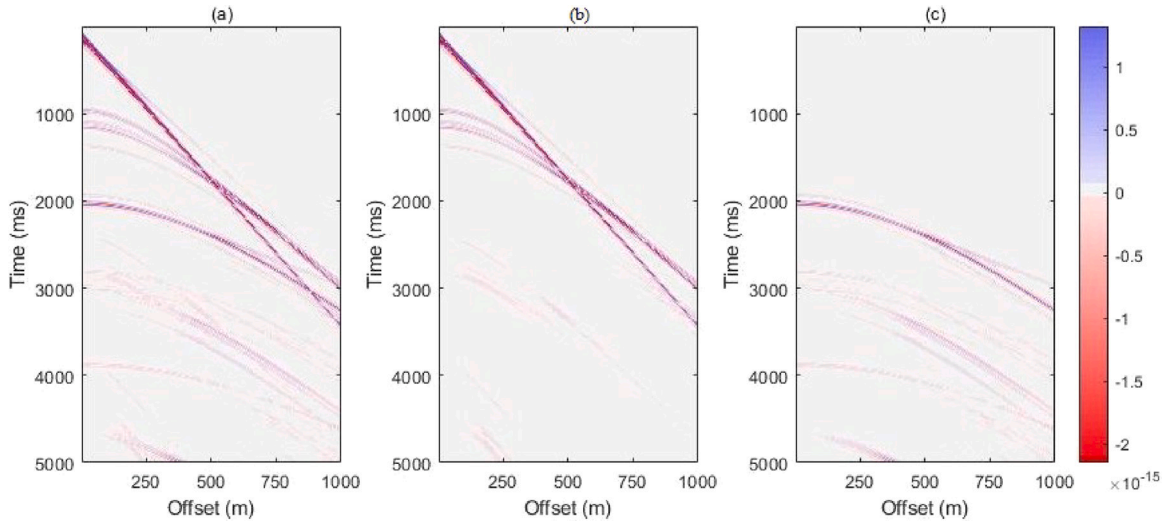

Fig. 14. Seismic records obtained with staggered-grid finite difference methods: (a) full model; (b) overburden model; (c) reservoir model obtained by subtracting the overburden from the full model.

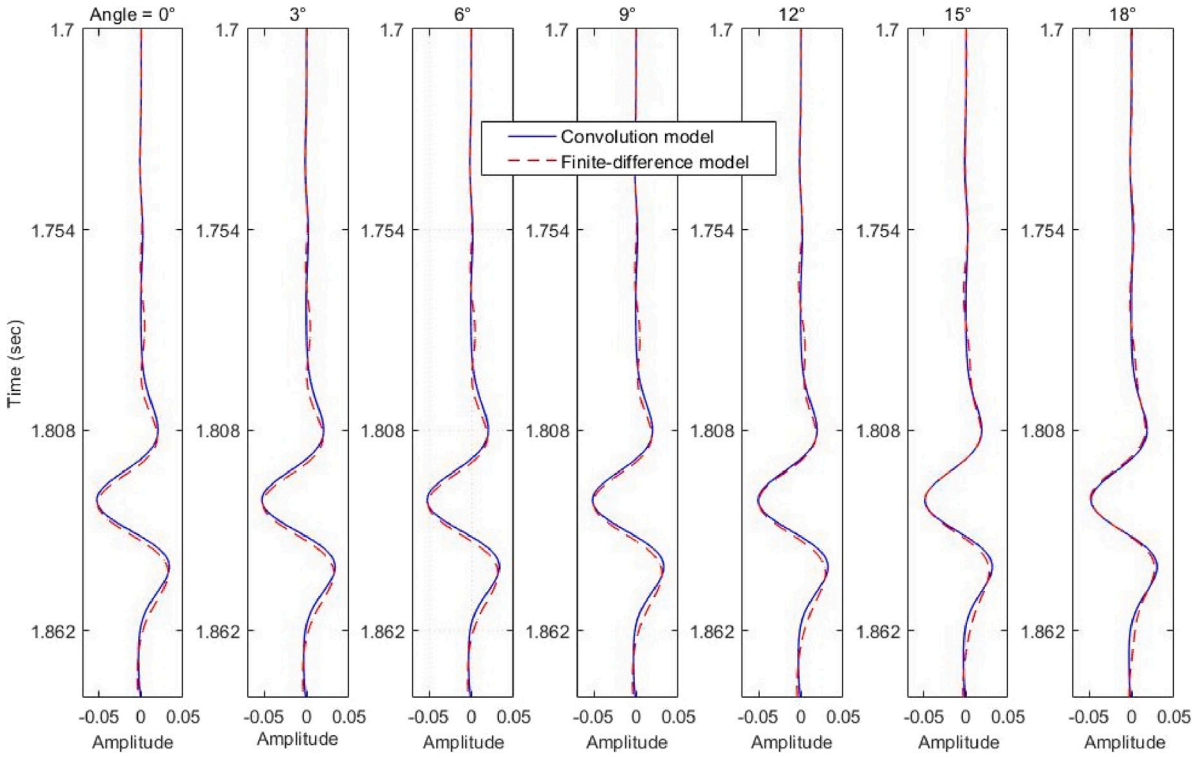

Fig. 15. Comparison between synthetic data modeled by using convolution and finite difference models after correcting the offset-dependent geometrical spreading.

models shows that the results are accurate (Fig. 8). Similarly, in the noise-added case, the results also show very good agreement with the true models (Fig. 9) and are consistent with the real models. However, the inverted results presented in Figs. 8 and 9 are after applying small weight Tikhonov regularization to the density and the shear wave velocity.

We then apply the inversion approach to a synthetic dataset built using the Edvard Grieg measured data along a section including horizontal and inclined stratigraphy and faulted geological layers. We adopt an elastic model obtained in previous studies (referred to as the true model in the following) to generate a synthetic seismic line. The seismic line comprises 38 common depth points (CDP) and the AVO inversion is applied trace by trace. The time window is from 500 to 2500 ms. Figs. 10–12 show the inversion results for P- and S-wave velocity and density, respectively. Each figure shows the comparison between the initial model, true model, and inverted results for all CDPs. For each model variable, we compute the RMS error between true and predicted models. The inversion shows accurate results for P-wave velocity, whereas density values are slightly under-predicted in the bottom part of the interval and S-wave velocity shows mismatched in the reservoir region. Fig. 13 shows the full stack of the seismic dataset, obtained after stacking the AVO gathers generated at each trace location, and the seismic response of the inverted model, showing an overall agreement between data and predictions. In some of the inversion results, the correlation between the predicted elastic properties is overestimated, possibly due to the linearization in the inverse problem.

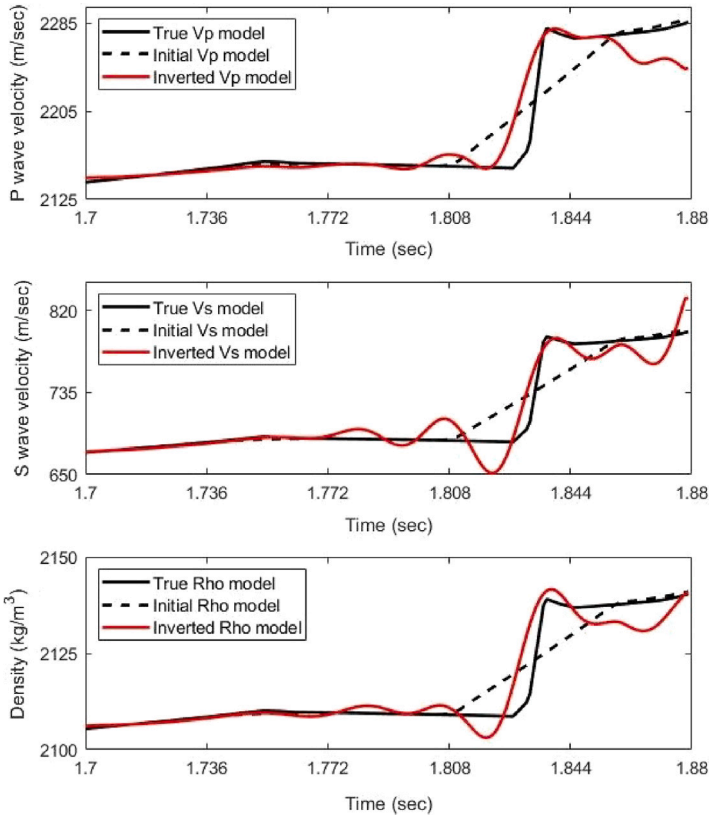

Fig. 16. Inverted P- and S-wave velocities (V_P, V_S) and density (ρ) at the top of the reservoir (1.7–1.88 s).

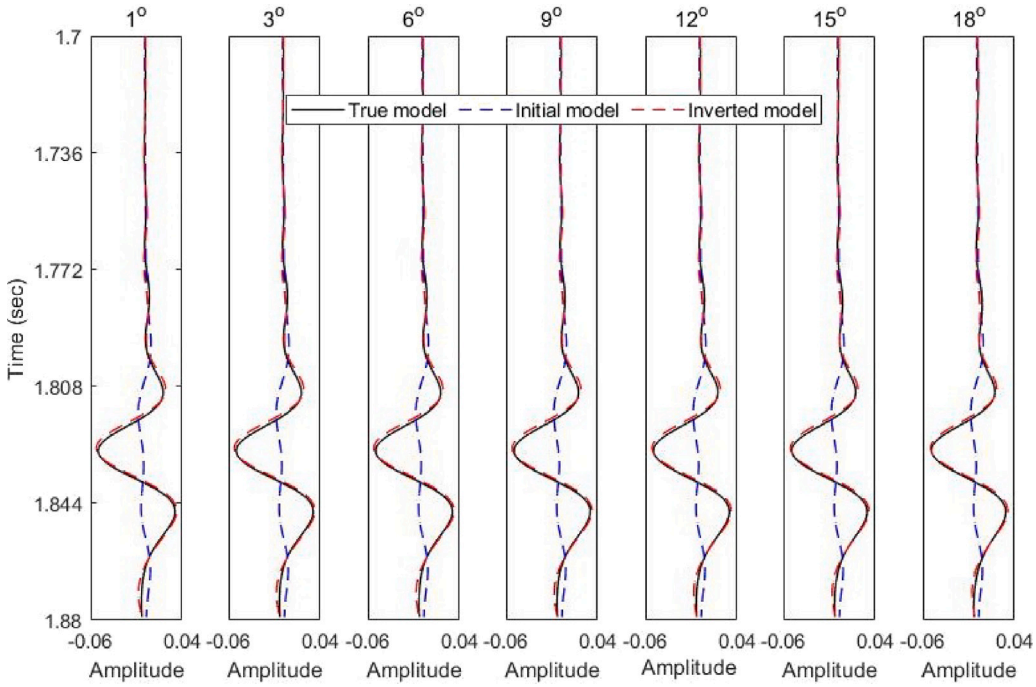

Fig. 17. Pre-stack amplitude versus angle (AVA) gathers based on true model simulated by staggered-grid finite difference method, initial model, and inverted model obtained with a convolutional approach.

This is a common effect in seismic and petrophysical inversion, due to the correlation of the seismic angles introduced in the processing which reduces the degrees of freedom of the solution and makes the problem underestimated.

We extend the inversion to a seismic dataset generated using the staggered-grid finite difference model of elastic waves. We first generate the synthetic seismic by computing the forward model for the entire section from the surface and extracting the reservoir layer between

1700 and 1888 ms. We perform normal moveout (NMO) correction offset-to-angle transformation and apply an amplitude scaling factor to remove the effects of offset-dependent geometrical spreading. The wavelet with a dominant frequency of 25 Hz is used for the FD model. We assumed a layered isotropic elastic medium with elastic properties given in Fig. 1 and simulate an OBC seismic survey. The number of receiver points are 1001 with a constant distance of 5 m, for a 5000 m maximum offset. The recording interval is 0.002 s. The synthetic seismograms generated by the finite difference simulations are shown in Fig. 14. The overburden layers extend to 1750 m, whereas the reservoir layer is between 1750 and 1940 m, such that the overburden reflections and associated interbedded multiples are subtracted from the model. The FD results at the top of the reservoir are shown in (Fig. 14c). As the staggered-grid finite difference modeling considers all the wave propagation effects, in order to implement a convolutional model-based inversion scheme for FD synthetic angles gathers, we have defined an amplitude scaling factor that compensates for the effects of geometrical spreading for FD seismic profiles and provides the best calibration between synthetics of both methods. The derivation of the amplitude scaling factor is described in Appendix B. The comparison between convolution and FD models at the reservoir zone level, after the application of the scaling factor, is shown in Fig. 15. We then run the inversion scheme assuming the FD model until incident angle 18°. The results of the proposed adjoint-state-based inversion applied to the staggered-grid FD model are shown in Figs. 16 and 17. Overall, the inverted P- and S- wave seismic velocities and density show good agreement with the true models, despite some discrepancies. Fig. 17 shows the synthetic angle gathers for the initial, true, and inverted models plotted trace by trace up to 18°, showing a good match.

4. Discussion

In the gradient descent-based optimization algorithms, it is necessary to compute the gradient equations of the least-square objective function with respect to unknown elastic variables. The efficiency of the algorithm relies on the accuracy and the effectiveness of the computation of the gradient. To efficiently and accurately compute the gradient, we adopt the adjoint-state technique. The adjoint-state variables do not depend on the perturbations of the model variables. We apply the method under the non-linear constraints and derive the set of gradient equations for the objective function. The advantage of using the adjoint-state method is that it only requires solving one additional linear system, which makes the inversion more efficient than the Fréchet derivative approach (Plessix, 2006). The optimization problem is then solved by using the L-BFGS optimizer of the non-linear quasi-Newton class based on the gradient computed with the adjoint-state method. The non-linear L-BFGS approximates the inverse Hessian matrix by using a few previous iterations ($l < 10$) and consequently reduces computational load and makes the algorithm more efficient than the traditional Newton–Raphson and Gauss–Newton methods. The proposed approach is tested on several examples based on two different forward models: the traditional convolutional approach and the FD method. The adjoint-state-based inversion method for the elastic properties can be theoretically applied to other properties e.g., seismic impedances, velocity ratio, or petrophysical parameters, by calculating the gradients with respect to the selected parameterization using the chain rule of derivative and by incorporating adequate rock-physics relations. The proposed inversion method can also be applied to other angle-dependent reflectivity operators such as Zoeppritz equations or their approximations (Shuey, 1985; Fatti et al., 1994)

5. Conclusions

We presented a non-linear seismic AVO inversion method based on a deterministic approach for the minimization of the objective function. The objective function is based on the convolutional model where the reflectivity is obtained using linearized Aki and Richards approximation. The gradient of the objective function is calculated by using the adjoint-state technique. The adjoint-state is computationally fast and more effective than traditional numerical methods. The minimization problem is iteratively solved by using L-BFGS, a non-linear optimization algorithm that approximates the inverse of Hessian and improves the convergence rate for inversion results. The applications of the proposed inversion scheme show accurate results for synthetic seismic data computed using the convolutional model as well as the staggered-grid finite difference method. The estimated synthetic angle gathers computed from the inversion results match the true data in both cases. The adjoint-state-based AVO inversion method can be applied to the different parameterizations of the model by using the chain rule of differentiation.

CRediT authorship contribution statement

Nisar Ahmed: Defined and developed the methodology, Implemented the code, Contributed to the writing. **Wiktor Waldemar Weibull:** Defined and developed the methodology, Contributed to the writing and coding. **Dario Grana:** Revised the methodology, Contributed to the writing.

Declaration of competing interest

The authors declare that they have no known competing financial interests or personal relationships that could have appeared to influence the work reported in this paper.

Acknowledgments

The authors would like to express gratitude to the Kunnskapsdepartementet and the National IOR Centre of Norway (led by the University of Stavanger) for the financial support of this project. The authors also acknowledge Lundin Energy Norway and their partners Wintershall Dea and OMW in the Edvard Grieg license for providing the seismic and well logs for this project. The authors are thankful to Patrick Connolly (Patrick Connolly Associates Ltd.) for reviewing and some good discussion about the paper. Nisar Ahmed is thankful to Tien Hoang Nguyen (Research Fellow at IER, UiS) for a nice discussion about the Edvard Grieg oil field and for helping to extract the 2D velocity model. The computations and simulations were performed on resources provided by UNINETT Sigma2 — the National Infrastructure for High-Performance Computing and Data Storage in Norway.

Code availability section

Name of the code/library: Non-linear AVO Inversion
Contact: ahmedseis23@gmail.com
Hardware requirements: Standard personal computer
Program language: MATLAB
Software required: MATLAB
The source codes are available for download at the link: https://github.com/nahmed215/avoinversion.git

Appendix A. Adjoint-state based gradients

The gradient ∇ of an objective function J given in the least-square Eq. (4), includes the partial derivatives of the objective function with respect to the model variables $m = [V_P(t),\ V_S(t),\ \rho(t)]$:

$$\nabla J = \left[\frac{\partial J(t)}{\partial V_P},\ \frac{\partial J(t)}{\partial V_S},\ \frac{\partial J(t)}{\partial \rho}\right] \tag{A.1}$$

Based on Eq. (4), the partial derivative of J are given by:

$$\frac{\partial J}{\partial V_P} = -\left[d - f(V_P,\ V_S,\ \rho)\right] \cdot \frac{\partial f}{\partial V_P} \tag{A.2}$$

$$\frac{\partial J}{\partial V_S} = -\left[d - f(V_P,\ V_S,\ \rho)\right] \cdot \frac{\partial f}{\partial V_S} \tag{A.3}$$

$$\frac{\partial J}{\partial \rho} = -\left[d - f(V_P,\ V_S,\ \rho)\right] \cdot \frac{\partial f}{\partial \rho} \tag{A.4}$$

In practical applications, elastic properties are discretized. We adopt the notation $V_P[i], V_S[i]$ and $\rho[i]$, for the value of velocity at a given interface i. In the discretized domain, the terms $\left(\frac{\partial f}{\partial V_P[i]}\right)$, $\left(\frac{\partial f}{\partial V_S[i]}\right)$ and $\left(\frac{\partial f}{\partial \rho[i]}\right)$ represent the Jacobian matrix and are given by

$$\frac{\partial f}{\partial V_P[i]} = -W * \frac{\partial R_{PP}(\theta)}{\partial V_P[i]} \tag{A.5}$$

$$\frac{\partial f}{\partial V_S[i]} = -W * \frac{\partial R_{PP}(\theta)}{\partial V_S[i]} \tag{A.6}$$

$$\frac{\partial f}{\partial \rho[i]} = -W * \frac{\partial R_{PP}(\theta)}{\partial \rho[i]} \tag{A.7}$$

We compute the gradient equations for each model variable using the adjoint method. In the AVO inverse problem, the Lagrangian function ($\mathcal{L}$) with the adjoint state variable λ is given by:

$$\mathcal{L}\left(V_P,\ V_S,\ \rho,\ R_{PP},\ \lambda\right) = \sum_i \int_\theta d\theta \left[d[i] - W[i] * R_{PP}[i]\right]^2 + \sum_i \int_\theta d\theta \left[R_{PP}[i] - A[i] \cdot \frac{\Delta\alpha}{\alpha} - B[i] \cdot \frac{\Delta\beta}{\beta} - C[i] \cdot \frac{\Delta\rho}{\rho}\right] \lambda_{[i]} \tag{A.8}$$

here,

$$A[i] = \left[\frac{1}{2}\left(1 + \tan^2\theta\right)\right] \qquad B[i] = \left[-\frac{4\beta[i]^2}{\alpha[i]^2} \cdot \sin^2\theta\right]$$

$$C[i] = \frac{1}{2}\left[1 - \frac{4\beta[i]^2}{\alpha[i]^2} \cdot \sin^2\theta\right]$$

while,

$$\alpha[i] = \frac{V_P[i+1] + V_P[i]}{2} \qquad \Delta\alpha[i] = V_P[i+1] - V_P[i]$$

$$\beta[i] = \frac{V_S[i+1] + V_S[i]}{2} \qquad \Delta\beta[i] = V_S[i+1] - V_S[i]$$

$$\rho[i] = \frac{\rho[i+1] + \rho[i]}{2} \qquad \Delta\rho[i] = \rho[i+1] - \rho[i]$$

The Lagrangian in Eq. (A.8) can be rewritten as $\mathcal{L} = \mathbf{J} + C * \lambda$, where C represents the constraints. The constraint in the Lagrangian multiplier is automatically satisfied if we compute R_{PP} using Aki and Richards equations as:

$$\left[R_{PP}[i] - A[i] \cdot \frac{\Delta\alpha}{\alpha} - B[i] \cdot \frac{\Delta\beta}{\beta} - C[i] \cdot \frac{\Delta\rho}{\rho}\right] = 0 \tag{A.9}$$

The gradient of the objective function $\boldsymbol{J}$ is achieved through the solution of the following system:

$$\frac{\partial \mathcal{L}}{\partial R_{PP}} = 0, \tag{A.10}$$

$$\frac{\partial \mathcal{L}}{\partial \lambda} = 0, \tag{A.11}$$

$$\begin{aligned}\frac{\partial \mathcal{L}}{\partial V_P[i]} = \int_\theta d\theta \Bigg\{ & \frac{A}{\alpha[i-1]} \cdot \lambda[i-1] - \frac{A}{\alpha[i]} \cdot \lambda[i] \\ & - \frac{A\Delta\alpha[i-1]}{2\alpha[i-1]^2} \cdot \lambda[i-1] - \frac{A\Delta\alpha[i]}{2\alpha[i]^2} \cdot \lambda[i] \\ & + \frac{4\beta[i-1]^2}{\alpha[i-1]^3} \cdot \sin^2\theta \cdot \frac{\Delta\beta[i-1]}{\beta[i-1]} \cdot \lambda[i-1] \\ & + \frac{4\beta[i]^2}{\alpha[i]^3} \cdot \sin^2\theta \cdot \frac{\Delta\beta[i]}{\beta[i]} \cdot \lambda[i] \\ & + \frac{2\beta[i-1]^2}{\alpha[i-1]^3} \cdot \sin^2\theta \cdot \frac{\Delta\rho[i-1]}{\rho[i-1]} \cdot \lambda[i-1] \\ & + \frac{2\beta[i]^2}{\alpha[i]^3} \cdot \sin^2\theta \cdot \frac{\Delta\rho[i]}{\rho[i]} \cdot \lambda[i] \Bigg\}\end{aligned} \tag{A.12}$$

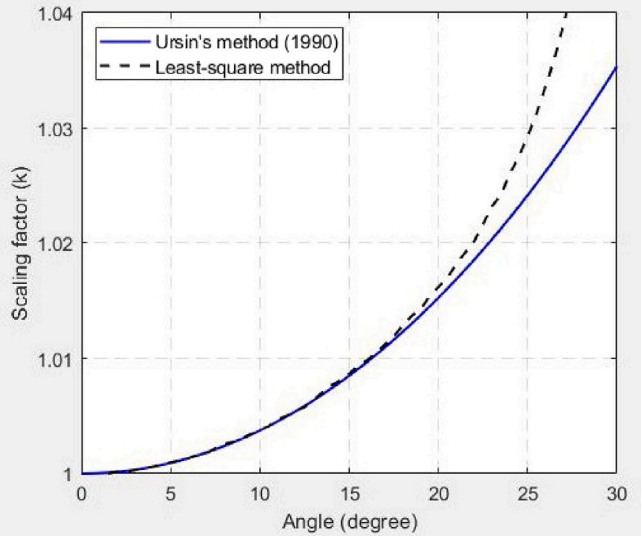

Fig. 18. The comparison between amplitude correction scaling factors to compensate for the effects of offset-dependent geometrical spreading. The least-square derived scaling factor shows a good correlation with Ursin's method (Ursin, 1990) up to incident angle 20°.

$$\begin{aligned}\frac{\partial \mathcal{L}}{\partial V_S[i]} = \int_\theta d\theta \Bigg\{ & -\frac{2\Delta\beta[i-1]}{\alpha[i-1]^2} \cdot \sin^2\theta \cdot \lambda[i-1] \\ & - \frac{2\Delta\beta[i]}{\alpha[i]^2} \cdot \sin^2\theta \cdot \lambda[i] \\ & - \frac{4\beta[i-1]}{\alpha[i-1]^2} \cdot \sin^2\theta \cdot \lambda[i-1] \\ & + \frac{4\beta[i]}{\alpha[i]^2} \cdot \sin^2\theta \cdot \lambda[i] \\ & - \frac{2\beta[i-1]}{\alpha[i-1]^2} \cdot \sin^2\theta \cdot \frac{\Delta\rho[i-1]}{\rho[i-1]} \cdot \lambda[i-1] \\ & - \frac{2\beta[i]}{\alpha[i]^2} \cdot \sin^2\theta \cdot \frac{\Delta\rho[i]}{\rho[i]} \cdot \lambda[i] \Bigg\}\end{aligned} \tag{A.13}$$

and

$$\begin{aligned}\frac{\partial \mathcal{L}}{\partial \rho[i]} = \int_\theta d\theta \Bigg\{ & C[i-1] \cdot \left(\frac{1}{\rho[i-1]}\right) \cdot \lambda[i-1] - C[i] \cdot \left(\frac{1}{\rho[i]}\right) \cdot \lambda[i] \\ & - C[i-1] \cdot \left(\frac{\Delta\rho[i-1]}{\rho[i-1]^2}\right) \cdot \lambda[i-1] - C[i] \cdot \left(\frac{\Delta\rho[i]}{\rho[i]}\right) \cdot \lambda[i] \Bigg\}\end{aligned} \tag{A.14}$$

When Eqs. (A.10) and (A.11) are satisfied, it means the derivatives of the extended objective function with respect to R_{PP} and state variable (λ) are zero. Then, the gradients of $\mathcal{L}$ and J with reference to the model properties coincide: $\frac{\partial \mathcal{L}}{\partial V_P[i]} = \frac{\partial J}{\partial V_P[i]}$, $\frac{\partial \mathcal{L}}{\partial V_S[i]} = \frac{\partial J}{\partial V_S[i]}$, and $\frac{\partial \mathcal{L}}{\partial \rho[i]} = \frac{\partial J}{\partial \rho[i]}$, and the Lagrangian can be used to find the derivative of J and obtain the gradient equations for $V_P[i]$, $V_S[i]$ and $\rho[i]$. The state variable λ can be computed as:

$$\lambda[i] = -2W[i] * (d[i] - W[i] * R_{PP}[i]) \tag{A.15}$$

Appendix B. Amplitude scaling factor

To compare the finite difference model and the convolution model, we define an amplitude scaling factor to compensate for the effect of offset-dependent geometrical spreading. If k is the scaling factor, the least-square equation can be written as:

$$\mathbf{J} = \frac{1}{2} \parallel \mathrm{d_C} - k \cdot \mathrm{d_{FD}} \parallel_t^2 \tag{B.1}$$

where d_C and d_{FD} stand for the convolution and the finite difference models computed for all the data for any travel time t. The derivative

of the discretized form ($t = 1, 2, 3, \ldots$) of Eq. (B.1) with respect to the scaling factor k the set equal to 0.

$$\frac{\mathrm{d}\mathbf{J}}{\mathrm{dk}} = -\sum_t \left((\mathrm{d_C} - k \cdot \mathrm{d_{FD}}) \cdot \mathrm{d_{FD}}\right) = 0 \tag{B.2}$$

which leads to

$$-\sum_t \mathrm{d_C} \cdot \mathrm{d_{FD}} + k \cdot \sum_t \mathrm{d_{FD}^2} = 0 \tag{B.3}$$

The scaling factor for the geometrical spreading can be then defined mathematically as:

$$k = \frac{\sum_t \mathrm{d_C} \cdot \mathrm{d_{FD}}}{\sum_t \mathrm{d_{FD}^2}} \tag{B.4}$$

The geometrical spreading scaling factor is plotted as a function of incident angles in Fig. 18. The comparison of the derived least-square based k is made with Ursin's method (Ursin, 1990) and the results displayed in Fig. 18 show the accuracy of the derived scaling factor up to the incident angle 20°.

References

Aki, K., Richards, P.G., 1980. Quantitative Seismology: Theory and Methods. The Maple-Vail Book Manufacturing Group USA.

Alessandrini, G., Maarten, V., Faucher, F., Gaburro, R., Sincich, E., 2019. Inverse problem for the Helmholtz equation with Cauchy data: Reconstruction with conditional well-posedness driven iterative regularization. ESAIM Math. Model. Numer. Anal. 53 (3), 1005–1030.

Assis, C.A., Schleicher, J., 2021. Introduction of the Hessian in joint migration inversion and improved recovery of structural information using image-based regularization. Geophysics 86 (6), R777–R793.

Aster, R.C., Borchers, B., Thurber, C.H., 2018. Parameter Estimation and Inverse Problems. Elsevier.

Azevedo, L., Grana, D., de Figueiredo, L., 2020. Stochastic perturbation optimization for discrete-continuous inverse problems. Geophysics 85 (5), M73–M83.

Biondi, E., Barnier, G., Clapp, R.G., Picetti, F., Farris, S., 2021. An object-oriented optimization framework for large-scale inverse problems. Comput. Geosci. 154, 104790.

Brossier, R., Operto, S., Virieux, J., 2010. Which data residual norm for robust elastic frequency-domain full waveform inversion? Geophysics 75 (3), R37–R46.

Broyden, C.G., 1970. The convergence of a class of double-rank minimization algorithms 1. general considerations. IMA J. Appl. Math. 6 (1), 76–90.

Buland, A., El Ouair, Y., 2006. Bayesian time-lapse inversion. Geophysics 71 (3), R43–R48.

Buland, A., Omre, H., 2003. Bayesian linearized AVO inversion. Geophysics 68 (1), 185–198.

Carcione, J.M., Kosloff, D., Kosloff, R., 1988. Wave propagation simulation in a linear viscoacoustic medium. Geophys. J. Int. 93 (2), 393–401.

Castagna, J.P., Batzle, M.L., Eastwood, R.L., 1985. Relationships between compressional-wave and shear-wave velocities in clastic silicate rocks. Geophysics 50 (4), 571–581.

Chiappa, F., Mazzotti, A., 2009. Estimation of petrophysical parameters by linearized inversion of angle domain pre-stack data. Geophys. Prospect. 57 (3), 413–426.

Constable, S.C., Parker, R.L., Constable, C.G., 1987. Occam's inversion: A practical algorithm for generating smooth models from electromagnetic sounding data. Geophysics 52 (3), 289–300.

Downton, J., 2005. Seismic Parameter Estimation from AVO Inversion (Ph.D. thesis). The University of Calgary, Calgary.

Downton, J.E., Ursenbach, C., 2006. Linearized amplitude variation with offset (AVO) inversion with supercritical angles. Geophysics 71 (5), E49–E55.

Dupuy, B., Romdhane, A., Nordmann, P.L., Eliasson, P., Park, J., 2021. Bayesian rock physics inversion: application to CO2 storage monitoring. Geophysics 86 (4), 1–73.

Epelle, E.I., Gerogiorgis, D.I., 2020. Adjoint-based well placement optimisation for Enhanced Oil Recovery (EOR) under geological uncertainty: From seismic to production. J. Pet. Sci. Eng. 190, 107091.

Evensen, G., et al., 2009. Data Assimilation: The Ensemble Kalman Filter. vol. 2, Springer.

Fatti, J.L., Smith, G.C., Vail, P.J., Strauss, P.J., Levitt, P.R., 1994. Detection of gas in sandstone reservoirs using AVO analysis: A 3-D seismic case history using the Geostack technique. Geophysics 59 (9), 1362–1376.

Faucher, F., Alessandrini, G., Barucq, H., de Hoop, M.V., Gaburro, R., Sincich, E., 2019. Full reciprocity-gap waveform inversion in the frequency domain, enabling sparse-source acquisition. arXiv preprint arXiv:1907.09163.

Feng-Qi, Z., Fu-Ji, W., Yan-Chun, W., Wei-Jun, W., Yan, L., 2013. Generalized linear AVO inversion with the priori constraint of trivariate cauchy distribution based on Zoeppritz equation. Chin. J. Geophys.-Chin. Ed. 56 (6), 2098–2115.

Fletcher, R., 1970. A new approach to variable metric algorithms. Comput. J. 13 (3), 317–322.

Gardner, G., Gardner, L., Gregory, A., 1974. Formation velocity and density—The diagnostic basics for stratigraphic traps. Geophysics 39 (6), 770–780.

Ghosh, S.K., 2000. Limitations on impedance inversion of band-limited reflection data. Geophysics 65 (3), 951–957.

Goldfarb, D., 1970. A family of variable-metric methods derived by variational means. Math. Comp. 24 (109), 23–26.

Golub, G.H., Van Loan, C.F., 2013. Matrix Computations. In: Johns Hopkins Studies in the Mathematical Sciences, Johns Hopkins University Press, Baltimore, MD.

Gouveia, W.P., Scales, J.A., 1997. Resolution of seismic waveform inversion: Bayes versus Occam. Inverse Problems 13 (2), 323.

Grana, D., 2020. Bayesian petroelastic inversion with multiple prior models. Geophysics 85 (5), M57–M71.

Hu, G.Q., Liu, Y., Wei, X.C., Chen, T.S., 2011. Joint PP and PS AVO inversion based on Bayes theorem. Appl. Geophys. 8 (4), 293–302.

Hu, J., Qian, J., Cao, J., Wang, X., Wang, H., Leung, S., 2021. Ray illumination compensation for adjoint-state first-arrival traveltime tomography. Geophysics 86 (5), 1–43.

Jin, S., Madariaga, R., 1994. Nonlinear velocity inversion by a two-step Monte Carlo method. Geophysics 59 (4), 577–590.

Kolbjørnsen, O., Buland, A., Hauge, R., Røe, P., Ndingwan, A.O., Aker, E., 2020. Bayesian seismic inversion for stratigraphic horizon, lithology, and fluid prediction. Geophysics 85 (3), R207–R221.

Kurt, H., 2007. Joint inversion of AVA data for elastic parameters by bootstrapping. Comput. Geosci. 33 (3), 367–382.

Lang, X., Grana, D., 2019. Rock physics modelling and inversion for saturation-pressure changes in time-lapse seismic studies. Geophys. Prospect. 67 (7), 1912–1928.

Le, H., Clapp, R.G., Levin, S.A., Biondi, B., 2020. A pipeline approach for three dimensional time-domain finite-difference multi-parameter waveform inversion on GPUs. Comput. Geosci. 140, 104503.

Levenberg, K., 1944. A method for the solution of certain non-linear problems in least squares. Quart. Appl. Math. 2 (2), 164–168.

Liu, X., Chen, J., Zeng, J., Liu, F., Huang, H., Zhao, Z., Luo, Y., 2021. An adaptive stratified joint PP and PS AVA inversion using accurate Jacobian matrix. Geophysics 86 (4), 1–145.

Liu, H., Li, J., Chen, X., Hou, B., Chen, L., 2016. Amplitude variation with offset inversion using the reflectivity method. Geophysics 81 (4), R185–R195.

Liu, D.C., Nocedal, J., 1989. On the limited memory BFGS method for large scale optimization. Math. Program. 45 (1), 503–528.

Luo, C., Ba, J., Carcione, J.M., Huang, G., Guo, Q., 2020a. Joint PP and PS pre-stack AVA inversion for VTI medium based on the exact Graebner equation. J. Pet. Sci. Eng. 194, 107416.

Luo, C., Ba, J., Carcione, J.M., Huang, G., Guo, Q., 2020b. Joint PP and PS pre-stack seismic inversion for stratified models based on the propagator matrix forward engine. Surv. Geophys. 41 (5), 987–1028.

Luo, X., Bhakta, T., Jakobsen, M., Nævdal, G., 2017. An ensemble 4D-seismic history-matching framework with sparse representation based on wavelet multiresolution analysis. SPE J. 22 (03), 985–1010.

Luo, C., Li, X., Huang, G., 2019. Pre-stack AVA inversion by using propagator matrix forward modeling. Pure Appl. Geophys. 176 (10), 4445–4476.

Luo, X., Stordal, A.S., Lorentzen, R.J., Nævdal, G., 2015. Iterative ensemble smoother as an approximate solution to a regularized minimum-average-cost problem: theory and applications. SPE J. 20 (05), 962–982.

Ma, X.Q., 2001. Global joint inversion for the estimation of acoustic and shear impedances from AVO derived P-and S-wave reflectivity data. First Break 19 (10).

Mallick, S., 1995. Model-based inversion of amplitude-variations-with-offset data using a genetic algorithm. Geophysics 60 (4), 939–954.

Mallick, S., 2007. Amplitude-variation-with-offset, elastic-impedence, and wave-equation synthetics—A modeling study. Geophysics 72 (1), C1–C7.

Marquardt, D.W., 1963. An algorithm for least-squares estimation of nonlinear parameters. J. Soc. Ind. Appl. Math. 11 (2), 431–441.

Maurya, S., Singh, K., Kumar, A., Singh, N., 2018. Reservoir characterization using post-stack seismic inversion techniques based on real coded genetic algorithm. J. Geophys. 39 (2).

Morozov, I.B., Ma, J., 2009. Accurate poststack acoustic-impedance inversion by well-log calibration. Geophysics 74 (5), R59–R67.

Nocedal, J., 1980. Updating quasi-Newton matrices with limited storage. Math. Comp. 35 (151), 773–782.

Pan, W., Innanen, K.A., Wang, Y., 2020. SeisElastic2D: An open-source package for multiparameter full-waveform inversion in isotropic-, anisotropic-and visco-elastic media. Comput. Geosci. 145, 104586.

Plessix, R.E., 2006. A review of the adjoint-state method for computing the gradient of a functional with geophysical applications. Geophys. J. Int. 167 (2), 495–503.

Rabben, T.E., Ursin, B., 2011. AVA inversion of the top Utsira Sand reflection at the Sleipner field. Geophysics 76 (3), C53–C63.

Ravasi, M., Vasconcelos, I., 2021. An open-source framework for the implementation of large-scale integral operators with flexible, modern high-performance computing solutions: Enabling 3D Marchenko imaging by least-squares inversion. Geophysics 86 (5), WC177–WC194.

Ricker, N., 1953. Wavelet contraction, wavelet expansion, and the control of seismic resolution. Geophysics 18 (4), 769–792.
Sengupta, M., Zhang, H., Zhao, Y., Jervis, M., Grana, Dario, 2021. Direct depth-domain Bayesian amplitude-variation-with-offset inversion. Geophysics 86 (5), M167–M176.
Shanno, D.F., 1970. Conditioning of quasi-Newton methods for function minimization. Math. Comp. 24 (111), 647–656.
Shaw, R., Srivastava, S., 2007. Particle swarm optimization: A new tool to invert geophysical data. Geophysics 72 (2), F75–F83.
Shuey, R., 1985. A simplification of the Zoeppritz equations. Geophysics 50 (4), 609–614.
Skopintseva, L., Ayzenberg, M., Landrø, M., Nefedkina, T., Aizenberg, A.M., 2011. Long-offset AVO inversion of PP reflections from plane interfaces using effective reflection coefficients. Geophysics 76 (6), C65–C79.
Tarantola, A., 1987. Inverse Problem Theory. Elsevier, New York.
Tarantola, A., 2005. Inverse Problem Theory and Methods for Model Parameter Estimation. SIAM.
Ursin, B., 1990. Offset-dependent geometrical spreading in a layered medium. Geophysics 55 (4), 492–496.
Virieux, J., 1986. P-SV wave propagation in heterogeneous media: Velocity-stress finite-difference method. Geophysics 51 (4), 889–901.
Xiao, S., Ba, J., Guo, Q., Carcione, J., Zhang, L., Luo, C., 2020. Seismic pre-stack AVA inversion scheme based on lithology constraints. J. Geophys. Eng. 17 (3), 411–428.
Zhao, L., Geng, J., Cheng, J., Han, D.h., Guo, T., 2014. Probabilistic lithofacies prediction from prestack seismic data in a heterogeneous carbonate reservoir. Geophysics 79 (5), M25–M34.
Zheglova, P., Malcolm, A., 2019. Vector acoustic full waveform inversion: taking advantage of de-aliasing and receiver ghosts. arXiv preprint arXiv:1910.05427.
Zhu, W., Xu, K., Darve, E., Beroza, G.C., 2021. A general approach to seismic inversion with automatic differentiation. Comput. Geosci. 151, 104751.
Zoeppritz, K., 1919. VIIb. Über Reflexion und Durchgang seismischer Wellen durch Unstetigkeitsfl. Göttinger Nachr. I, 66–84.